Journal of Engineering Mechanics and Machinery (2026)
Clausius Scientific Press, Canada

DOI: 10.23977/jemm.2026.110115
ISSN 2371-9133 Vol. 11 Num. 1

Measurement and Validation of High-Temperature Mechanical Parameters of TC4 Titanium Alloy Using Digital Image Correlation and Finite Element Simulation

Zefang Zhao, Huafeng Li, Yingli Zhu*

School of Mechanical Engineering, Tianjin University of Science and Technology, Tianjin, China
**Corresponding Author*

Keywords: DIC, TC4 Titanium Alloy, Mechanical Parameter Measurement, Finite Element Simulation

Abstract: A combined experimental and simulation approach was employed to investigate the mechanical properties of TC4 titanium alloy at elevated temperatures. A high-temperature tensile testing system integrated with digital image correlation (DIC) technology was established to conduct tensile tests at nine temperatures ranging from 26 ℃ to 750 ℃. True stress–strain curves were obtained, from which key mechanical parameters—including elastic modulus, yield strength, tensile strength, Poisson's ratio, strain hardening exponent (n-value), and plastic strain ratio (r-value) were derived. The results reveal that as temperature increases, elastic modulus, yield strength, and tensile strength decrease significantly, whereas Poisson's ratio increases, indicating enhanced plastic deformation capability. Both the n-value and r-value exhibit an overall decreasing trend, reflecting reduced resistance to plastic instability and thinning. Furthermore, finite element simulations were performed and the simulated stress–strain responses were in good agreement with the experimental results. The developed temperature–displacement coupling model effectively validates the reliability of the experimental measurements and parameter calculations.

1. Introduction

TC4, also known as Ti-6Al-4V, is a common titanium alloy composed of elements such as titanium, aluminum, and vanadium [1-4]. TC4 is a lightweight alloy with high strength and good corrosion resistance. This material has good high-temperature resistance and is widely used in aero-engine components, chemical equipment, and high-temperature electronic components [5-7]. High-temperature tensile tests were conducted on TC4 specimens, and their mechanical parameters were measured and calculated. The strain hardening index (n value) and plastic strain ratio (r value) were analyzed. The n value is an important parameter representing the cold deformation of the material and has a significant impact on the stamping performance of the material and the quality of the stamped parts. It reflects the ability of the metal material to resist further plastic deformation at a certain deformation rate and is an indicator of the strain hardening performance of the metal material [8-9]. The r value is an important parameter for evaluating the deep drawing performance

of thin metal sheets, reflecting the ability of thin metal sheets to resist thinning or thickening when subjected to tensile or compressive forces in a certain plane [10-11]. The n-value and r-value have become important indicators for evaluating the forming performance of materials. Therefore, it is of great significance to study the mechanical parameters of TC4 plates at high temperature and the variation law of n-value and r-value for their performance and the improvement of processing technology.

At present, there are many difficulties in the calculation of high temperature mechanical parameters, especially n-value and r-value in engineering. For example, the experiment may be affected by factors such as experimental equipment error and non-uniformity of sample preparation; the selection of fitting algorithm and the determination of parameters may affect the final result [12]. When there are multiple stages in the curve, it is also a challenge to determine the fitting range; the processing of experimental data, especially in non-uniform strain fields, may require the use of appropriate data smoothing and filtering techniques. It is even more difficult to measure the stress and strain data of specimens in high temperature environment.

In order to calculate the mechanical parameters of the material, it is necessary to measure the strain change of the material in various directions. The traditional contact measurement method usually cannot work in high temperature environment. Therefore, by performing non-contact measurement of the deformation of TC4 material, the existing problems in the experiment can be solved. Digital image processing technology (DIC) is a non-contact, non-interference, full-field deformation detection technology based on image processing. It uses a digital camera to collect spots on the surface of the object to be inspected, and then processes the captured images to obtain the deformation of the sample [13-14]. For example, Feng [15] et al. used DIC and SEM to investigate the micromechanical properties and deformation mechanisms of 3D-printed TC4/TC11 gradient titanium alloys. Results show superior tensile properties, with fracture occurring on the TC4 side, and heterogeneous deformation-induced strengthening identified as the key strengthening mechanism in the gradient zone. Wang [16] et al. proposed an SPH-FEM coupling method to predict the hypervelocity impact performance of composite protective structures (CPS) for spacecraft, validated through aluminum plate multi-shock shield tests. Results show the method effectively evaluates impact performance via projectile energy curves, demonstrating improved computational efficiency and suitability for braid-filled CPS under hypervelocity impact conditions. Zhao [17] et al. studied the effect of Al content in magnesium alloy on strain hardening behavior under room temperature conditions. The results showed that as the Al content increased, the n value of the material showed a trend of first increasing and then decreasing, and reached a peak in the Mg-3Al state. Gu [18] et al. proposed to use digital image correlation technology to measure the r value of the material in the elongation stage after necking. Huang [19] et al. applied DIC to accurately measure r-values in multiple directions for cold-rolled high-strength sheet steels, overcoming the limitations of conventional extensometer methods. Results show that incorporating DIC-measured r-values into the Hill-48 anisotropic model yields significantly better simulation accuracy than the isotropic von-Mises model, confirming DIC as a superior approach for characterizing anisotropic deformation behavior. Yue [20] et al. investigated the hot compression deformation behavior of as-cast TC21 titanium alloy in the β single-phase region across varying temperatures (1273–1473 K), strain rates (0.1–10 s^{-1}), and height reductions. Results reveal that flow stress exhibits steady-state characteristics, while at a strain rate of 10 s^{-1}, dynamic recrystallization significantly alters the strain hardening exponent, and both strain rate sensitivity and strain hardening exponents change dramatically once strain exceeds the critical value of 0.5–0.55.

This paper uses a combination of experimental and simulation methods to conduct tensile tests on TC4 titanium alloy at different temperatures and uses DIC to measure the displacement, strain

and other data of the material in different directions to obtain the real stress-strain curve. The elongation after fracture, reduction of area, yield strength, tensile strength, elastic modulus, Poisson's ratio and n value and r value of the material are calculated and the influence of temperature rise on the mechanical parameters of the material is summarized. Finally, the temperature-displacement coupling model in finite element simulation is used to verify the accuracy of the experimental results.

2. Experiment and Method

2.1. Sample Preparation

The sample material used in this paper is TC4 titanium alloy plate produced by Baoji Titanium Industry. This material is highly representative among titanium alloys, and its elemental composition is shown in Table 1.

Table 1: Chemical composition of TC4 titanium alloy.

Elemental composition	Ti	Al	V	Fe	C	N	H	O
content(%)	margin	6.11	3.93	0.13	0.02	<0.005	<0.001	0.11

The material dimensions were manufactured according to GB/T 228.2-2015. Because DIC measurements were to be performed on the material under high temperature conditions, a speckled spray coating with high-temperature resistant paint was required. First, the specimen was sanded to remove surface impurities, then different colors of high-temperature resistant paint were sprayed alternately to form irregular speckles, as shown in Figure 1. The high-temperature resistant paint used in this experiment has a maximum withstand temperature of 1200℃, which meets the maximum temperature requirement of the experiment.

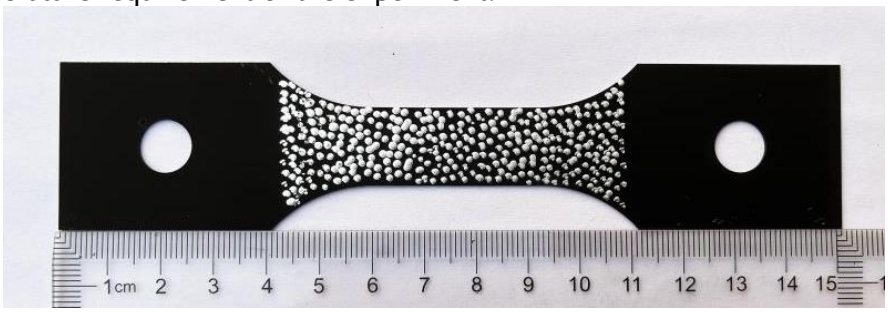

Figure 1: Surface speckle pattern applied for digital image correlation measurement.

2.2 Test Methods

Tensile tests were conducted according to GB/T 228.1-2010 "Metallic Materials - Tensile Testing - Part 1: Tests at Room Temperature" and GB/T 228.2-2015 "Metallic Materials - Tensile Testing - Part 2: Tests at High Temperature". The test equipment consisted of the MTS Landmark 370.10 high-precision hydraulic servo system and digital imaging technology (DIC) measuring equipment from MTS Corporation, USA. An electric heating furnace and thermocouples were also used to record temperature changes. The assembled test setup is shown in Figure 2.

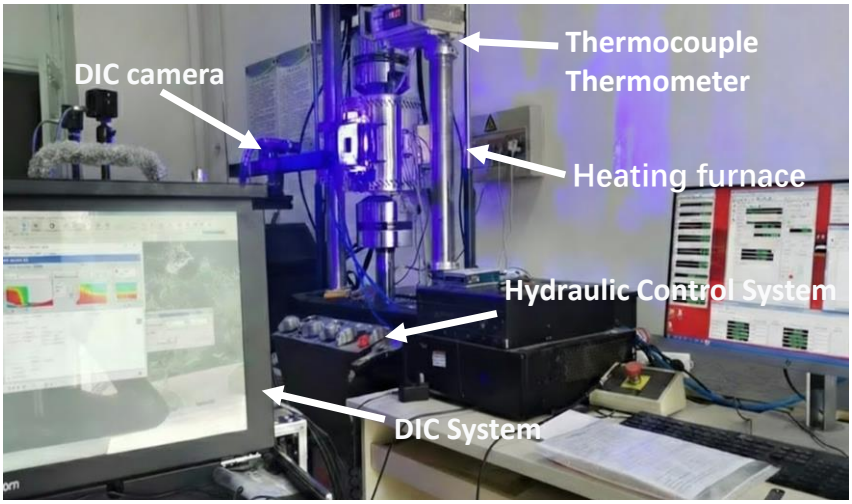

Figure 2: Experimental setup for high-temperature tensile testing with the DIC measurement system.

Nine temperature groups (26℃, 100℃, 150℃, 200℃, 250℃, 300℃, 350℃, 700℃, and 750℃) were used as controls. First, the sample was placed on the testing machine, and the furnace was heated to the required temperature. After holding at this temperature for 10 minutes, the test began. During this time, the DIC device was adjusted to the optimal shooting angle. After the test started, the sample was stretched at a speed of 0.14 mm/min until the elastic phase ended, then stretched at a speed of 3 mm/min until fracture. The entire process was recorded using the DIC at a frequency of 1 second per frame. The acquired images were then processed, the required analysis area was selected, and the full-field strain was calculated using the DIC. The strain in the x and y directions was calculated using virtual extensometers, as shown in Figure 3. It can be seen that the strain in the image shows a decreasing trend from the center to both sides. Two mutually perpendicular virtual extensometers were selected in the area of highest strain concentration, and the acquired data was exported to calculate the true stress and strain of the material.

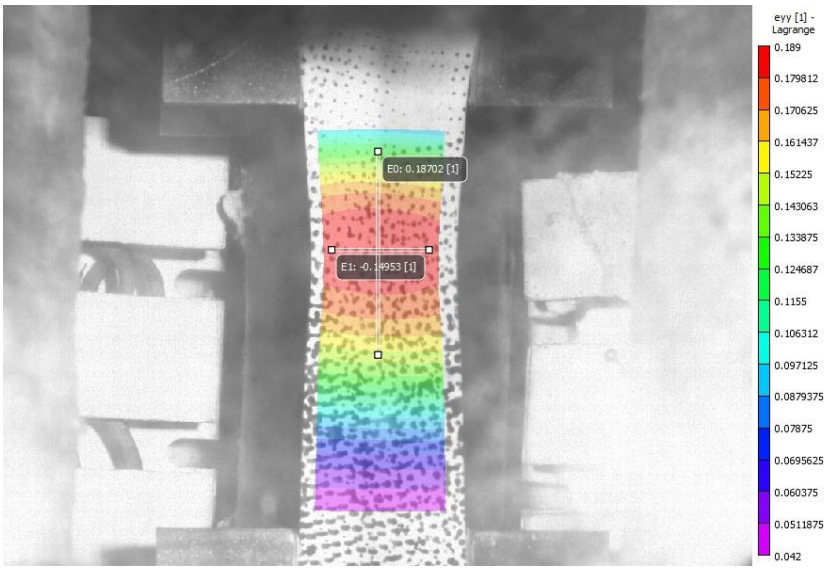

Figure 3: Macroscopic morphology of tensile specimens after deformation.

3. Experimental Principle

This paper calculates the elastic modulus and Poisson's ratio of materials according to

GB/T22315-2008. The elastic modulus, also known as Young's modulus, represents the ratio of the restoring force to the strain of a material under tension within the elastic range. It is represented by the symbol E and can be expressed by formula (1). Poisson's ratio represents the ratio of the expansion of a material in one direction after being compressed in another direction. It is one of the indicators of the isotropy and anisotropy of a material and is represented by the symbol μ. Its expression can be expressed by formula (2).

$$E=\sigma/\varepsilon \tag{1}$$

$$\mu= -\varepsilon_x/\varepsilon_y \tag{2}$$

Where σ represents tensile stress, ε represents tensile strain, ε_x represents strain in the x-direction, and ε_y represents strain in the y-direction.

The tensile strength, yield strength, elongation after fracture, and reduction of area of materials are calculated according to the GB/T 228.1-2021 standard. Tensile strength, denoted by R_m, represents the resistance to maximum uniform plastic deformation of a material and reflects its fracture resistance. Yield strength refers to the limit at which a metallic material can resist minor plastic deformation, the so-called "restraint," denoted by $R_{p0.2}$. Elongation after fracture is the percentage of the length the specimen elongates relative to its original length when the material fractures under tensile force, denoted by A. Reduction of area is the percentage of the maximum length a material specimen can reach before tensile fracture relative to its original length, denoted by Z. Their mathematical expressions are as follows.

$$R_m = F_b/S_0 \tag{3}$$

$$R_{p0,2} = F_e/S_0 \tag{4}$$

$$A = \frac{L_1-L_0}{L_0} \times 100\% \tag{5}$$

$$Z = \frac{S_0-S_1}{S_0} \times 100\% \tag{6}$$

Where F_b is the maximum force at yield, F_e is the constant force at yield, L_1 is the gauge length after tension, L_0 is the original gauge length, S_1 is the cross-sectional area of the fracture surface, and S_0 is the original cross-sectional area.

According to GB/T 5028-2008, the plastic strain index n is calculated and defined as the true plastic strain index in the mathematical equation of the true stress and true plastic strain under uniaxial tensile stress. This expression can be represented by formula (7):

$$s = C \times e^n \tag{7}$$

$$\ln s = \ln C + n \ln e \tag{8}$$

Where: s is the true stress, e is the true plastic strain, and C is the strength coefficient.

The slope of the straight line in the double logarithmic coordinate plane is the strain hardening index, and the calculated result is rounded to 0.01 according to GB/T 8170.

The plastic strain ratio r is calculated according to GB/T 5027-2016. The changes in length and width at a specified plastic strain level are tested. The true plastic strain of the specimen length and the true plastic strain of the specimen width are calculated using formula (9) and (10) respectively (elastic deformation is removed by default in the formulas):

$$\varepsilon_1 = \ln\left(\frac{L_0+\Delta L}{L_0} - \frac{F}{S_0 \times m_g}\right) \tag{9}$$

$$\varepsilon_b = \ln\left(\frac{b_0+\Delta b}{b_0} - \frac{\mu \times F}{S_0 \times E}\right) \tag{10}$$

In the formula (10): E is the elastic modulus, μ is Poisson's ratio; L_0 is the original length of the specimen, ΔL is the instantaneous change in length; S_0 is the original cross-sectional area; b_0 is the original width of the specimen; Δb is the instantaneous change in width.

To obtain a better r value, the plastic deformation range is selected with the actual plastic strain of length as the horizontal axis and the actual plastic strain of width as the vertical axis. The slope m_r of the fitted straight line is obtained, and the r value is calculated using formula (11). The result is then rounded to 0.05.

$$r = -\frac{m_r}{1+m_r} \tag{11}$$

4. Results Analysis

4.1 Tensile Results

Six specimens were selected for each temperature as a group. Tensile data were processed according to GB/T 228 standard after the test. The stress-strain curves obtained from each group were basically consistent. Therefore, one specimen from each group was selected as an example to plot the curve. The actual stress-strain curves from 26℃ to 750℃ are shown in Figure 4. It can be seen that before 700℃, the curves of the material in the early elastic stage are basically overlapping. As the temperature increases, the stress required for the material to enter the plastic stage decreases, and the maximum force required during the tensile process also decreases, indicating that the material softens. This is most obvious above 700℃, with almost no elastic stage. There is no obvious yield stage in the entire tensile process, especially at higher temperatures. With further increase in load, the plastic stage curve is relatively smooth, and there are significant differences in tensile strength at different test temperatures. Subsequently, it gradually enters the local deformation stage until the specimen fractures.

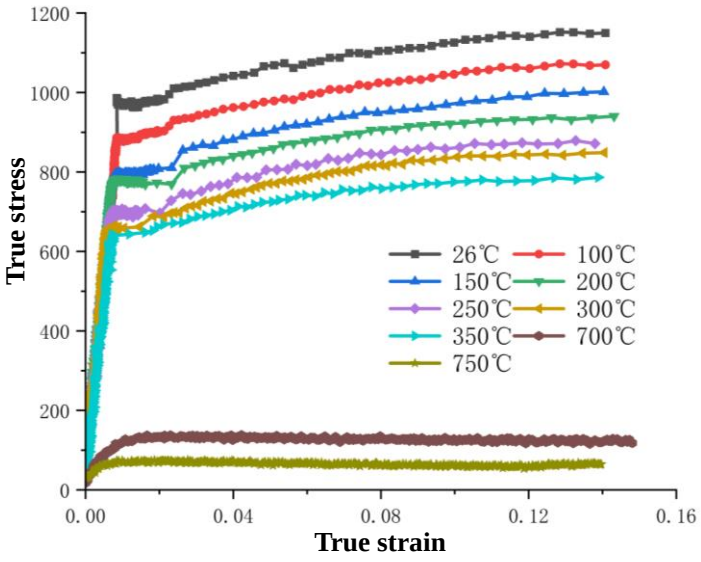

Figure 4: True stress-strain curve.

Based on the actual stress-strain curves and data collected by DIC, the mechanical parameters of TC4 titanium alloy at different temperatures can be obtained according to the mathematical formulas in this paper. The average value of each group of specimens is taken as the result, as shown in Table 2.

Table 2: Mechanical parameters of TC4 at different temperatures.

Temperature/℃	A/%	Z/%	E/GPa	μ	Rp0.2/MPa	Rm/MPa
26	18.1	29.2	110	0.28	870	966
100	20.7	30.1	100.4	0.29	817	910
150	22.1	31.9	95.6	0.30	756	866
200	24.7	33.4	91.4	0.32	715	805
250	25.6	34.8	88.9	0.32	678	751
300	19.4	30.3	82.3	0.34	603	714
350	16.7	28.4	77.9	0.34	570	682
700	224.9	85.1	8.9	0.35	115	114
750	292.3	88.7	5.1	0.36	66.4	86

Figure 5 shows the trend of parameter variation with temperature. As can be seen from Figure 5(a), the elongation after fracture Z and the reduction of area A of the material generally show an increasing trend with increasing temperature, but decrease at 300℃ and 350℃, and reach their maximum values at 700℃ and 750℃, where the material undergoes severe deformation. The elongation after fracture A does not change significantly before 350℃, but changes significantly after 700℃; the reduction of area Z shows a trend of first increasing and then decreasing before 350℃. As shown in Figure 5(b), the elastic modulus, yield strength, and tensile strength of the material all decrease with increasing temperature, reaching their lowest point at 750℃. This demonstrates that temperature has a significant impact on both the elasticity and plasticity of the material. At 750℃, the material almost reaches a failure state, with the elastic modulus, yield strength, and tensile strength all reaching their minimum values. Figure 5(c) shows that the Poisson's ratio of the material continuously increases with increasing temperature, from 0.28 at 26℃ to 0.36 at 750℃. This indicates that as the temperature increases, the material becomes less hard, softer, and weaker, making it more prone to plastic deformation.

Based on the actual stress and strain values, the n and r values are calculated. n is the slope of the logarithmic fitted line between the actual plastic strain and the actual stress, and r is the slope of the fitted line between the actual width plastic strain and the actual length plastic strain. The specific values are then calculated using the formula.

The n and r values for each group are calculated and averaged. The results are shown in Table 3. It can be seen that both n and r values gradually decrease with increasing temperature. To more intuitively illustrate the changing pattern, a line graph of the n and r values is plotted as shown in Figure 6. The n value gradually decreases, dropping to approximately 0.04 at 750℃; the r value fluctuates before 700℃, and then shows a rapid decreasing trend after 700℃. A more detailed analysis follows.

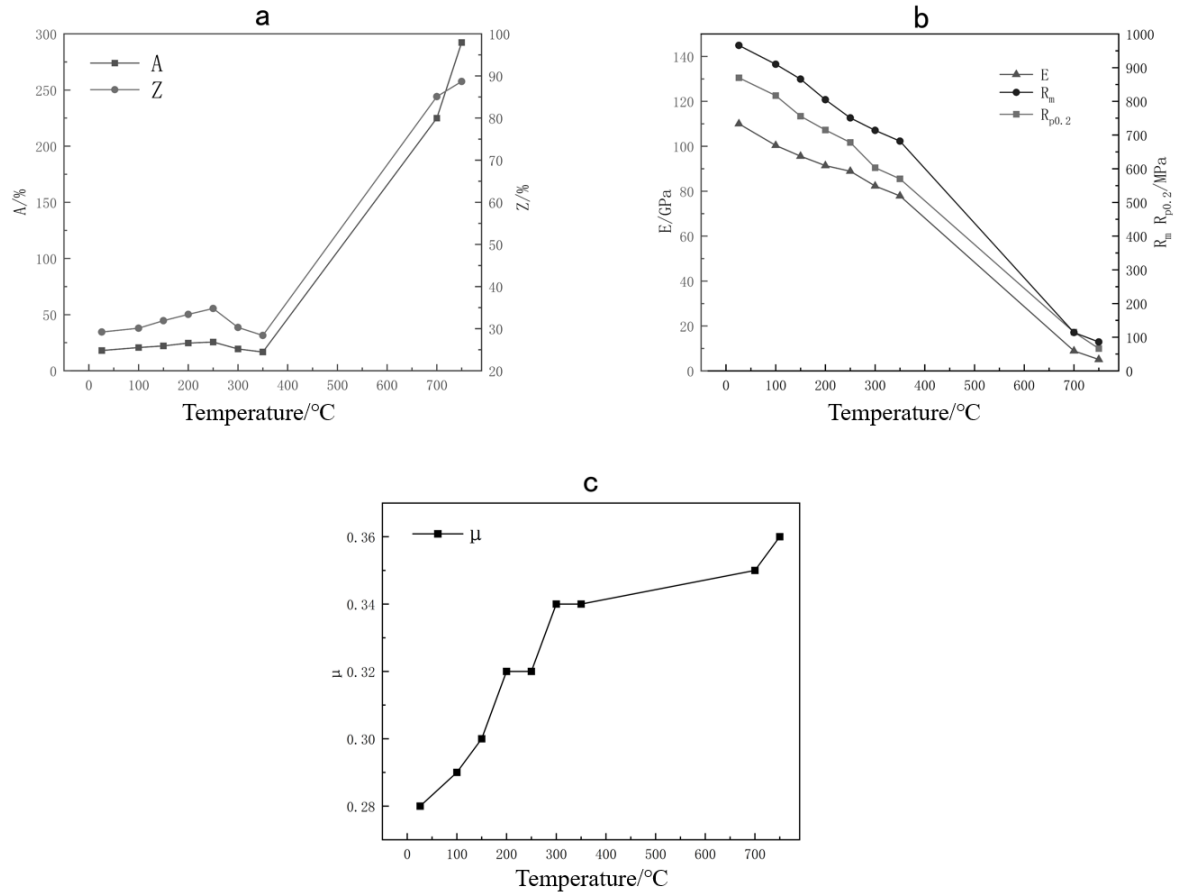

Figure 5: Mechanical parameters vary with temperature.

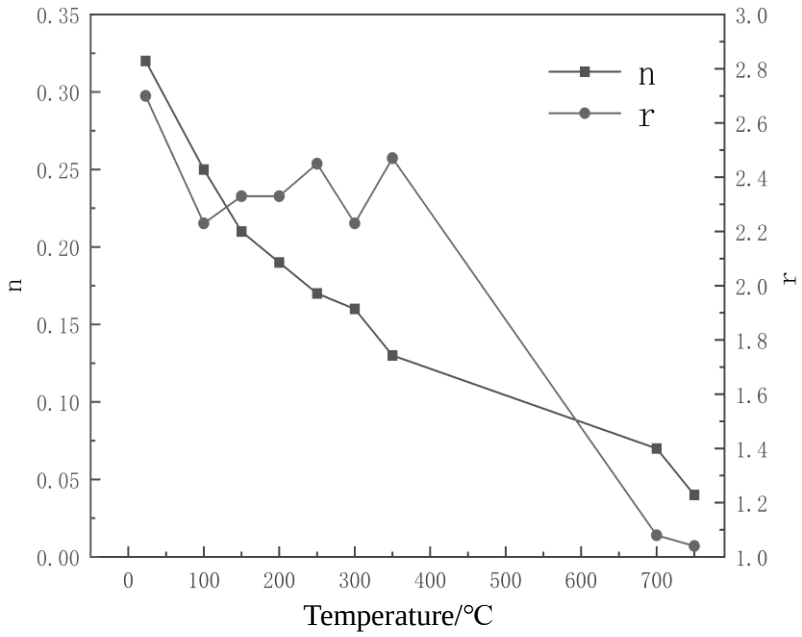

Figure 6: The variation of n and r values with temperature.

The line graph shows that the n-value of the material decreases with increasing temperature. The

decrease is rapid before 200℃, slows down between 200-350℃, and finally drops to around 0.04 at 750℃. This indicates that the resistance of TC4 to plastic deformation decreases with increasing temperature, and the rate of hardness increase is relatively slow with increasing strain. The r-value decreases before 100℃, fluctuates around 2.4 between 100-350℃, and continues to decrease after 700℃, dropping to around 1 at 750℃. This indicates that the material's resistance to instability and thinning generally decreases with increasing temperature, but remains relatively constant between 100-350℃. Between 700 ℃ and 750 ℃, it exhibits isotropic properties, but the r-value is generally greater than 1, indicating good stamping performance.

4.2 Result Verification

Because the values of n and rare affected by many factors, the experimental accuracy is required to be high. In order to verify the accuracy of the experimental results, Abaqus software was used to perform simulation and compare the simulated values with the experimental values. Temperature and velocity-related material properties were imported. The material temperature was assigned by defining the initial temperature field.

To concisely illustrate the simulation process and the comparison between the model and experimental results, four temperatures (100℃, 200℃, 350℃, and 700℃) were selected for comparison. The simulation results were plotted as real stress-strain curves, and compared with the experimental results as shown in Figure 7. It can be seen that the real stress-strain curves of the simulation results basically coincide with the experimental results under the four temperature conditions. Due to the uneven temperature distribution, limitations in material processing accuracy, and errors in DIC data recording during the experiment, the stress-strain curves under the experimental conditions will show slight fluctuations and some errors in accuracy compared with the simulation results. At 700℃, the experimental data showed larger fluctuations due to the loading rate, but the overall trend was consistent with the simulation data. Compared with the experimental data, the simulation curve was smoother, with an overlap rate of 90%, which indicates that the uniaxial tensile simulation model can simulate real tensile experiments well.

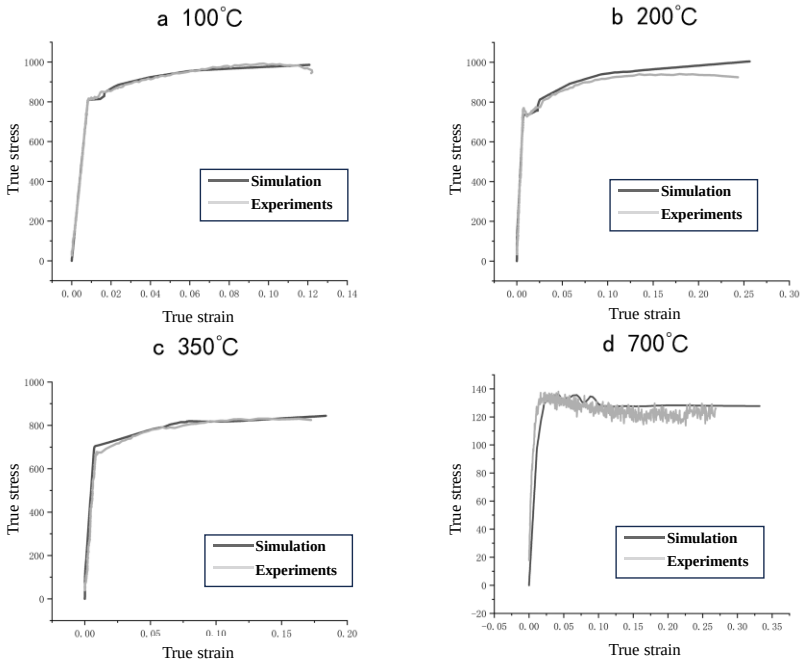

Figure 7: Comparison of simulation and experimental results.

To calculate the specific n and r values, the measured data needs to be fitted. The n value is calculated using the ratio curve of ln n to ln s, and the r value is calculated using the true plastic strain in the length direction and the true plastic strain in the width direction. To better illustrate the calculation process, data at 100℃ is used as an example. The slope of the fitted curve represents the required n and r values. The comparison between the simulation data and the experimental data after fitting is shown in Figure 8. The slope of the simulated n value is 0.02 larger than the experimental value, indicating a shift in the figure. The curves for the r value have a high degree of overlap, with a difference of 0.03 calculated by the formula. Neither deviation exceeds 0.05.

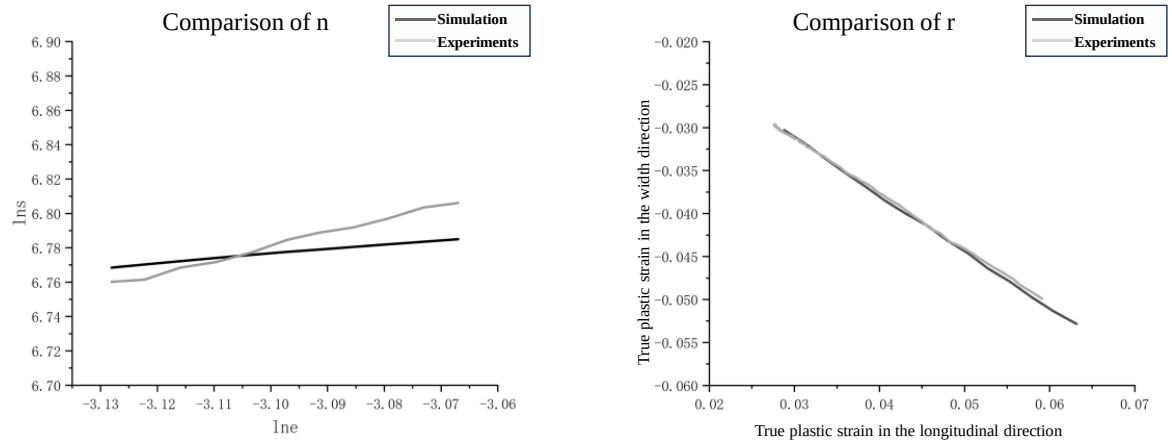

Figure 8: Simulation and testing values of n and r at 100 ℃.

Table 3 shows the comparison of n and r values at all temperatures. It can be seen that as the temperature increases, the trend of the simulated n value is basically the same as the experimental result, with the largest deviation at 100℃, reaching 0.02. The simulated r value also does not deviate significantly from the experimental result, reaching a maximum of 0.03 at 100℃. Due to various factors, the experimental values and simulation values of the actual stress-strain curve at 100℃ deviated to some extent. The n and r values were extremely sensitive to small changes in the data, resulting in the largest deviation at 100℃, but all were less than 0.05, which is within an acceptable range. This proves the reliability of the obtained n and r values.

Table 3: The values of n and r at all temperatures.

Temperature/℃	Exp. n-value	Sim. n-value	Exp. r-value	Sim. r-value
23	0.32	0.32	2.70	2.71
100	0.25	0.27	2.23	2.26
150	0.21	0.22	2.33	2.32
200	0.19	0.20	2.33	2.33
250	0.17	0.17	2.45	2.40
300	0.16	0.16	2.23	2.21
350	0.13	0.12	2.47	2.46
700	0.07	0.07	1.08	1.11
750	0.04	0.05	1.04	1.04

5. Conclusion

(1) As the temperature increases, the elastic modulus, yield strength, and tensile strength of TC4

titanium alloy all decrease, reaching their minimum values at 750℃. This indicates that increasing temperature affects both the elastic and plastic properties of the material, and at 750℃, it almost completely loses its original properties. Poisson's ratio increases with increasing temperature, increasing by nearly 29% at 750℃, indicating that the material becomes increasingly soft and less hard with increasing temperature, and its strength decreases, making it more prone to plastic deformation.

(2) The strain hardening exponent n of TC4 material gradually decreases with increasing temperature, decreasing from approximately 0.32 at room temperature to approximately 0.04 at 750℃. This indicates that increasing temperature weakens the material's resistance to uniform plastic deformation, making it more susceptible to plastic deformation. The plastic strain ratio r shows a trend of first decreasing, then remaining constant, and finally decreasing again. It decreases slowly before 100℃ and significantly decreases between 350-750℃, indicating that the material's resistance to instability and thinning generally decreases with increasing temperature, but remains relatively stable between 100-350℃.

(3) The temperature-displacement coupling model in ABAQUS can obtain the true stress-strain curve of TC4 with increasing temperature, and it matches well with the experimental data, verifying the accuracy of the n and r values. This demonstrates that ABAQUS simulation can correctly verify the changes in the mechanical parameters of TC4 with increasing temperature.

References

[1] Peng, X., Guo, H., Wang, T. and Yao, Z. (2012) Effects of β treatments on microstructures and mechanical properties of TC4-DT titanium alloy. Materials Science and Engineering: A, 533, 55-63.

[2] Zhao, Z., Ji, H., Zhong, Y., Han, C. and Tang, X. (2022) Mechanical properties and fracture behavior of a TC4 titanium alloy sheet. Materials, 15(23), 8589.

[3] Li, G. R., Li, Y. M., Wang, F. F. and Wang, H. M. (2015) Microstructure and performance of solid TC4 titanium alloy subjected to the high pulsed magnetic field treatment. Journal of Alloys and compounds, 644, 750-756.

[4] Zhang, H., Li, J., Ma, P., Xiong, J. and Zhang, F. (2018) Study on microstructure and impact toughness of TC4 titanium alloy diffusion bonding joint. Vacuum, 152, 272-277.

[5] Wang, M., Chen, X., Dai, F., Peng, K., Singh, R. A. and Konovalov, S. (2023) Simulation of residual stress and micro-plastic deformation induced by laser shock imprinting on TC4 titanium alloy aero-engine blade. Journal of Materials Research and Technology, 26, 9419-9436.

[6] Miao, X., Hong, H., Peng, J., Ping, T., Fengfeng, B. and Chenyang, J. (2023) Study on mixed-mode fracture behavior of TC4 titanium alloy. Theoretical and Applied Fracture Mechanics, 125, 103911.

[7] Wang, H., Zhao, K., Chu, X., Zhao, B. and Gao, J. (2019) Constitutive modelling and microscopic analysis of TC4 alloy sheet at elevated temperature. Results in Physics, 13, 102332.

[8] Naderi, M., Ketabchi, M., Abbasi, M. and Bleck, W. (2011) Analysis of microstructure and mechanical properties of different high strength carbon steels after hot stamping. Journal of Materials Processing Technology, 211(6), 1117-1125.

[9] Zhu, Y., Wang, Q., Huang, Z., Qin, L., Li, Z. and Ma, L. (2022) Strain hardening exponent and strain rate sensitivity exponent of cast AZ31B magnesium alloy. Metals, 12(11), 1942.

[10] Briesenick, D. and Liewald, M. (2024) Efficient net shape forming of high-strength sheet metal parts by Transversal Compression Drawing. The International Journal of Advanced Manufacturing Technology, 130(5), 3053-3063.

[11] Kim, I. S., Nam, S. K. and Lee, D. N. (2017) Plastic Strain Ratio of Warm and Hot Asymmetrically Rolled AA6061 Al Sheet. Applied Mechanics and Materials,873, 60-64.

[12] El Fazani, H., Coil, J., Chamberland, O. and Laliberte, J. (2022) Determination of experimental uncertainties in tensile properties of additively manufactured polymers using the GUM method. Measurement, 202, 111726.

[13] Sun, Z., Lyons, J. S. and McNeill, S. R. (1997) Measuring microscopic deformations with digital image correlation. Optics and Lasers in Engineering, 27(4), 409-428.

[14] Meng, S., Li, J., Liu, Z., Wang, W., Niu, Y. and Ouyang, X. (2021) Study of flexural and crack propagation behavior of layered fiber-reinforced cementitious mortar using the digital image correlation (DIC) technique. Materials, 14(16), 4700.

[15] Feng, X., Chen, J., Lin, X., Zhang, X., Wang, Y. and Sun, C. (2024) Microdeformation and strengthening mechanism of 3D printed TC4/TC11 gradient titanium alloy subjected to tensile loading. Materials Science and

Engineering: A, 915, 147265.
[16] Wang, Y., Li, Q., Xu, Y., Zhou, J., Li, Y., Zhang, D. and Jiang, D. (2025) Prediction of hypervelocity impact performance of composite protective structures using a combined finite element method and smoothed particle hydrodynamics approaches. Journal of Mechanical Science and Technology, 39(2), 553-566.
[17] Zhao, C., Chen, X., Wang, J., Tu, T., Dai, Y., Shin, K. S. and Pan, F. (2019) Strain hardening behavior in Mg–Al alloys at room temperature. Advanced Engineering Materials, 21(3), 1801062.
[18] Gu, G. H., Kim, Y., Seo, M. H. and Kim, H. S. (2023) A method for measuring plastic strain ratio over a wide strain range using the digital image correlation technology. Metals and Materials International, 29(7), 1880-1884.
[19] Huang, G., Yan, B. and Xia, Z. (2011) Measurement of r-values of high strength steels using digital image correlation. SAE International Journal of Materials and Manufacturing, 4(2011-01-0234), 385-395.
[20] Yue, Z., Zhu, Y., Fan, J. and Shao, Z. (2019) The strain rate sensitivity exponent and the strain hardening exponent of as-cast TC21 titanium alloy in β single-phase region. Materials Research Express, 6(11), 1165g1.